A 3D FDTD Thin-wire Model of Single-core Coaxial Cables with Multiple Conductive Layers

Binghao Li[1], Yaping Du[1], Mingli Chen[1] and Zhe Li[2]

[1]Dept. of Building Services Engineering, The Hong Kong Polytechnic University, Hung Hom, Kowloon, Hong Kong
[2]China Southern Power Grid Company Limited, Shenzhen Power Supply Bureau, Shenzhen, China

***Abstract* — In this paper, a thin-wire model of single-core coaxial cables with 3 or more conductive layers is proposed for transient analysis using the finite-difference time-domain (FDTD) method. The multilayer cable is regarded as a series of 2-conductor coaxial transmission lines. The currents in these lines can be, however, unbalanced, and may not return via earth, such as in the case of a direct lightning strike. The FDTD method is employed to evaluate electromagnetic coupling outside the cable. Frequency-dependent surface impedances of conductors are fully considered using the Bessel functions. They are integrated into the time-domain analysis with a vector fitting technique. Updating equations for both lossless and lossy cables are derived. The proposed model is validated TLT analytically and with the traditional FDTD method numerically. Good agreements are observed. Finally, the proposed model is applied to analyze the transients in a cable connection station under a direct lightning strike.**

***Keywords* — Coaxial cable, multilayer conductors, thin wire, FDTD, frequency-dependent loss**

I. INTRODUCTION

Underground power cables have been extensively used in electric power systems, especially in urban areas and across water bodies [1] due to their better appearance, smaller voltage drops and less probability of fault occurrence. Transient simulations for underground cables during lightning strikes or under system fault conditions are necessary and inevitable, given the high capital cost [2]. Single-core coaxial cables with multiple conductive layers are one of the common types of underground cables. To facilitate time-domain transient simulations in the system, a 3D FDTD model for such cables is investigated in this paper.

The EM field propagation in multilayer and multiconductor cables has been well investigated with the 1D discrete transmission line theory [3], Electromagnetic Transients Program (EMTP) [4, 5] and 1D FDTD method [6, 7]. The frequency-dependent loss of the cables was considered by using the rational functions in the frequency domain [8-10] or approximated directly in the time domain [11-13]. The coupling between cables and fields was investigated in [14-16] analytically and in [17-20] numerically. While EMTP is based on the circuit theory in that components can only be connected electrically. It is troublesome for EMTP to consider interactions between the non-uniform electromagnetic field and transmission lines [21], and lines without a current return path.

The 3D finite-difference time-domain (FDTD) method, proposed by Yee firstly in 1966 [22], offers an alternative approach for solving electromagnetic problems in the time domain. After 1990, with the unpredictable development of computer science technology, the 3D FDTD method has been developed as one of the mainstream simulation techniques for solving theoretical and practical EM problems. The FDTD method has the advantages of broadband field simulation, less memory space, easy implementation of parallel computing and others. To simulate a wire conductor accurately, the traditional 3D FDTD method needs to discretize the wire structure with extremely dense mesh, which will reduce calculation efficiency significantly. A thin-wire model without conductor meshing on its cross section is an approach for solving the problem. Traditional thin-wire models [23-26] mimicking long wire structures have been successfully applied to analyze electromagnetic transients in power systems. Examples can be found for grounding systems [27], high voltage substations [28], overhead lines [29-31], transmission towers [32], vertical conductors [33, 34], light rail systems [35] and lines with corona discharge [36].

Several advanced thin-wire models for single-core cables have also been proposed recently to improve the computation efficiency of the FDTD method. In [37] the loss of a conductor is modeled with the frequency-dependent surface impedance calculated with Bessel functions. In [38, 39], the vector fitting technique is used for solving transient interaction problems with the surface impedance concept. In [40], the cable model for two co-centric conductors is proposed by integrating the transmission line theory (TLT) and the FDTD method. An extended model is further developed in [41, 42] by taking into account the skin effect in the cables. It is noted that these models can only simulate single-core cables with two metallic layers.

Compared with the cable with two metallic layers, maintaining stability performance and calculation efficiency for cables with multiple conductive layers is a big challenge. There is no existing model that can simulate a lossy cable with multiple conductive layers in a 3D FDTD environment. In this paper, a stable, matrix-free and efficient thin-wire model is proposed to simulate such a cable using a series of 2-conductor transmission lines. Currents in conductive layers can be unbalanced, and may not return via a

conductive path, such as in the case of a direct lightning strike. The FDTD method is employed to evaluate electromagnetic coupling outside the cable. The frequency-dependent losses are fully considered using Bessel functions. They are integrated into time-domain analysis with a vector fitting technique. In Section II, the equations of both lossless and lossy cables are introduced. The model validation is discussed in Section III. The proposed thin-wire model is validated with the transmission line theory (TLT) analytically and the traditional FDTD method numerically. Finally, the proposed model is applied to analyze the transients in a cable connection station under a direct lightning strike.

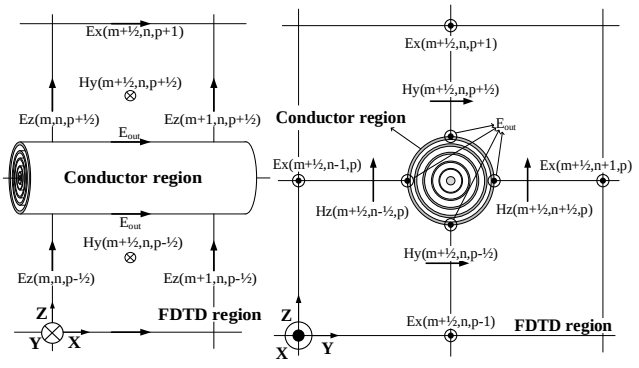

(a) x-z plan view (b) y-z plan view

Fig. 1 Configuration of FDTD/conductor regions in the working volume (m, n and p denote cell indices in x, y and z directions, and q denotes time step index)

II. SINGLE-CORE CABLES WITH MULTILAYER CONDUCTORS

Similar to the thin wire model in [41], the whole working volume is divided into two regions: conductor region and FDTD region, as shown in Fig. 1. Fig. 1 shows the configuration of one single-core cable with multiple conductive layers for transient analysis. In the FDTD region, electromagnetic fields outside the cable are evaluated with the corrected updating equations [26]. Current and voltage propagated along the cable are simulated in the conductor region using the TLT. In the FDTD simulation, the conductor region is regarded as a thin wire. During each updating procedure, the updating information is exchanged between two regions, such as the total conductor current (from the FDTD region to conductor region) and cable voltages at terminals and surface current density of the cable (from the conductor region to FDTD region).

Without loss of generality, a single-core cable with three co-centric conductors is selected for the description of the proposed thin-wire model. This cable consists of core A, sheath B and armor C, and two insulation layers (layer AB and layer BC). Fig. 2 (a) shows the configuration and geometric parameters of the cable, as well as currents in the conductors. In the conductor region, two 2-conductor coaxial transmission lines are constructed, i.e., (i) the one made of conductors A and B, and (ii) the one made of conductors A/B and C. In the transmission line (ii), as shown in Fig. 2 (b), conductors A and B are grouped together and are treated as a single wire carrying current I_{AB} (I_{AB}=I_A + I_B). Therefore, the multiple transmission line equations are reduced to a series of classical 2-conductor transmission line equations. Note that the currents in each transmission line may not be balanced, i.e., $I_A + I_B \neq 0$ or $I_{AB} + I_C \neq 0$.

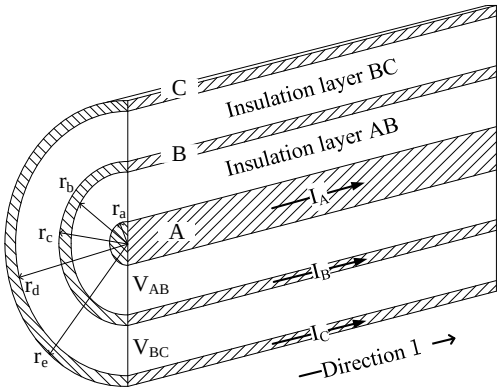

(a) Three conductors

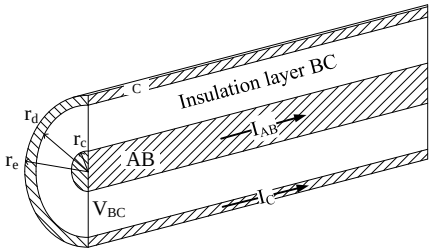

(b) Equivalent two conductors

Fig. 2 Configurations of single-core cables with 2 and 3 co-centric conductors

With total current I_t ($I_t = I_{AB} + I_C$) obtained in the FDTD region by integrating H field components, I_{AB} and I_C are determined using the transmission line equations in the transmission line (ii). Subsequently, I_A and I_B are obtained using the equations for the transmission line (i). The updating procedure for a lossless cable is relatively straightforward. It is described first, followed by the one for a lossy cable. Given the primary frequency of a lightning current, most extruded insulations in cables are practically lossless [44, 45]. The shunt admittance of insulations in cables is considered as frequency-independent in the analysis.

A. *Updating procedure for the lossless cable*

The one-dimensional wave equations for both transmission lines (a) and (b) with the pairs of unbalanced currents I_A and I_B, I_{AB} and I_C are described by

$$-\frac{\partial V_{AB}}{\partial l} = sL_{AB} \cdot I_A$$
$$-\frac{\partial I_A}{\partial l} = sC_{AB} \cdot V_{AB} \quad (1)$$

$$-\frac{\partial V_{BC}}{\partial l} = sL_{BC} \cdot I_{AB}$$
$$-\frac{\partial I_{AB}}{\partial l} = sC_{BC} \cdot V_{BC} \quad (2)$$

in the s-domain, where per-unit length inductance and capacitance are given in Table 1. In Table 1, $\varepsilon_{r.AB}$ and $\mu_{r.AB}$ are the relative permittivity and permeability of the material in insulation layer AB, and $\varepsilon_{r.BC}$ and $\mu_{r.BC}$ are the relative permittivity and permeability of the material in layer BC. Note that the currents in the outer conductors of the lines do not appear in these transmission line equations. The unbalanced current in the cable does not necessarily return via earth.

Table 1 Inductance and Capacitance of two Transmission lines

Inductance	$L_{AB}=\frac{\mu_0\mu_{r,AB}}{2\pi}\ln\frac{r_b}{r_a}$	$L_{BC}=\frac{\mu_0\mu_{r,BC}}{2\pi}\ln\frac{r_d}{r_c}$
Capacitance	$C_{AB}=2\pi\varepsilon_0\varepsilon_{r,AB}\Big/\ln\frac{r_b}{r_a}$	$C_{BC}=2\pi\varepsilon_0\varepsilon_{r,BC}\Big/\ln\frac{r_d}{r_c}$

Now we have the space-time discretization of (1) and (2) with the same step sizes as those adopted in the FDTD region. The updating equations for currents in the conductor region then are given by

$$\begin{aligned} I_{AB}^{q} &= I_{AB}^{q-1}-\frac{\Delta t}{L_{BC}}\frac{\Delta V_{BC}^{q-1/2}}{\Delta l} \\ I_{A}^{q} &= I_{A}^{q-1}-\frac{\Delta t}{L_{AB}}\frac{\Delta V_{AB}^{q-1/2}}{\Delta l} \end{aligned} \tag{3}$$

where Δt is the time step, and Δl is the segment length. The superscript q denotes the index of the time step. Both I_C and I_B then are determined by

$$\begin{aligned} I_{C}^{q} &= I_{t}^{q}-I_{AB}^{q}, \\ I_{B}^{q} &= I_{AB}^{q}-I_{A}^{q}. \end{aligned} \tag{4}$$

The current updating in the conductor region is synchronized with the H field updating in the FDTD region.

Similarly, voltage updating in the conductor region is synchronized with the E field updating in the FDTD region. voltages are updated half time step later than currents and are given by

$$\begin{aligned} V_{AB}^{q+1/2} &= V_{AB}^{q-1/2}-\frac{\Delta t}{C_{AB}}\frac{\Delta I_{A}^{q}}{\Delta l}, \\ V_{BC}^{q+1/2} &= V_{BC}^{q-1/2}-\frac{\Delta t}{C_{BC}}\frac{\Delta I_{AB}^{q}}{\Delta l}. \end{aligned} \tag{5}$$

Since the cable is lossless, the surface E field on the outer surface of conductor C is identical to zero. The E field components along the cable in the FDTD region then is enforced to zero in the next FDTD updating step [41].

B. Updating procedure for the lossy cable

In the case of a lossy cable, voltage drops arising from surface impedances of both inner and outer conductors in a need to be considered. The transmission line equations presented in (1) and (2) then are modified to be

$$\begin{aligned} -\frac{\partial V_{AB}}{\partial l} &= \left(sL_{AB}+Z_{a.A}-Z_{b.A}\right)I_A-Z_{b.B}I_B \\ -\frac{\partial I_A}{\partial l} &= sC_{AB}V_{AB} \end{aligned} \tag{6}$$

for transmission line (i), and

$$\begin{aligned} -\frac{\partial V_{BC}}{\partial l} &= \left(sL_{BC}-Z_{d.AB}\right)I_{AB}+Z_{c.A}I_A+Z_{c.B}I_B-Z_{d.C}I_C \\ -\frac{\partial I_{AB}}{\partial l} &= sC_{BC}V_{BC} \end{aligned} \tag{7}$$

for transmission line (ii), where $Z_{x,Y}$ denotes the surface impedance on surface x contributed by the current in conductor Y. For example, $Z_{c,A}$ is the surface impedance on the surface at $r=r_c$ contributed by current I_A. Surface impedances of a coaxial cable can be expressed using the Bessel functions, and are listed in Appendix A.

Surface impedances in (6) and (7) are frequency-dependent. They cannot be directly used in the time-domain simulation. In this paper, frequency-dependent parameters are approximated as rational functions with the vector fitting technique [46, 47]. The rational function is expressed as

$$Z_{x.Y}(s)=d_{x.Y}+sh_{x.Y}+\sum_{m=1}^{N}\frac{r_{x.Y.m}}{s-a_{x.Y.m}}, \tag{8}$$

where $d_{x,Y}$ and $h_{x,Y}$ represent a constant component and a differential component, and $a_{x,Y.\mathrm{m}}$ and $r_{x,Y.\mathrm{m}}$ are poles and residues of the rational function. These rational functions are invoked in the time-domain simulation using a convolutional technique.

Similar to (3), the discrete transmission line equations (6) and (7) with the rational functions given in (8) can be derived, and are presented in Appendix B. With total current I_t passed from the FDTD region, I_{AB} is calculated first in the conductor region. Substitute (4) in (7), the updating equation for I_{AB} in the time domain can be derived, and is given in (B1) in Appendix B. Note, I_A and I_B are not updated yet at this updating step. In order to estimate the conductor loss on the surface of Conductor C, we assume $I_A^q \approx I_A^{q-1}$ and $I_B^q \approx I_B^{q-1}$. It is observed in Section III-B that this assumption will not introduce a noticeable error. I_C can then be updated with (4). Substitute (4) in (6), the updating equation for I_A can be derived, is given in (B2). Finally, I_B of a lossy cable can be updated using (4).

Unlike the lossless cable, E_{out}, the E field on the outer surface of Conductor C is not equal to zero. It is determined by the currents in all conductors and is expressed in s-domain as

$$E_{out}(s)=Z_{e.AB}\cdot I_{AB}+Z_{e.C}\cdot I_C\,. \tag{9}$$

The discrete version of the updating equation for E_{out} in the time domain is given in (B3). Voltage differences over two insulation layers can be updated with (5) since the shunt conductance of insulation is ignored. The time step for both

FDTD region and the thin-wire model is the same. Both voltage and current in the cable are updated together with E/H fields in the FDTD region.

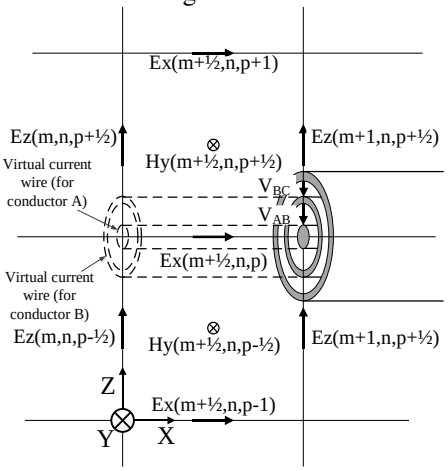

Fig. 3 Configuration of a terminal of a single-core cable structure

C. *Special arrangements at the cable terminals*

To obtain discrete equations of (3), the cable is divided into M current segments and M+1 voltage segments along the axial direction in the conductor region. Note, voltage and current segments are offset by half segment length. And voltage segments 1 and M+1 are located at two opposite ends of the cable. Both transmission line voltage V_{AB} and V_{BC} at two end segments are included as the integral of the E field for updating the H field in the FDTD region. Take a cable running in the *x* direction as an example, as shown in Fig. 3. The updating equation of Hy components is expressed as

$$H_y^{q+1}(m+1/2,n,p+1/2)=H_y^{q}(m+1/2,n,p+1/2)-\frac{\Delta t}{\mu\Delta z}\cdot \left[\begin{matrix}E_x^{q+1/2}(m+1/2,n,p+1)\\ -E_x^{q+1/2}(m+1/2,n,p)\end{matrix}\right]+\frac{\Delta t}{\mu\Delta x}\left[\begin{matrix}E_z^{q+1/2}(m,n,p+1/2)-\\ E_z^{q+1/2}(m+1,n,p+1/2)\end{matrix}\right] -\frac{\Delta t}{\mu\Delta x\Delta z}\left(V_{AB}^{q+1/2}+V_{BC}^{q+1/2}\right), \tag{9}$$

where Δx and Δz are cell sizes in the *x* and *z* directions. *m*, *n* and *p* are the indexes of space steps in the *x*, *y* and *z* directions.

Virtual current wires are added to the end of the cable, and connected to the inner conductors (conductors A and B). They are placed at the same location as shown in Fig. 3. These wires are used for 1) updating terminal transmission line voltages V_{AB} and V_{BC} with (5), and 2) connecting external wires to the cable. The total segment current is calculated by summing up currents of these wires. Assume, for instance, that there are 5 external wires connected to the cable terminal from different directions in the FDTD region. External wires 1 and 2 are connected to the conductor A via one virtual wire, wires 3 and 4 to conductor B via another virtual wire, and the 5th wire to the armor directly. The virtual wire currents $I_{Vir.A}$ and $I_{Vir.B}$ of conductors A and B are calculated as,

$$\begin{aligned} I_{Vir.A} &= I_{Ext.1}+I_{Ext.2}\\ I_{Vir.B} &= I_{Ext.3}+I_{Ext.4}\end{aligned}. \tag{10}$$

where $I_{Ext.i}$ (i=1…5) is the current in external wire *i*. There is no extra procedure for connecting the 5th wire and the armor. If the terminals of conductor A or B are left open, the currents in the additional segments are set to be zero [48].

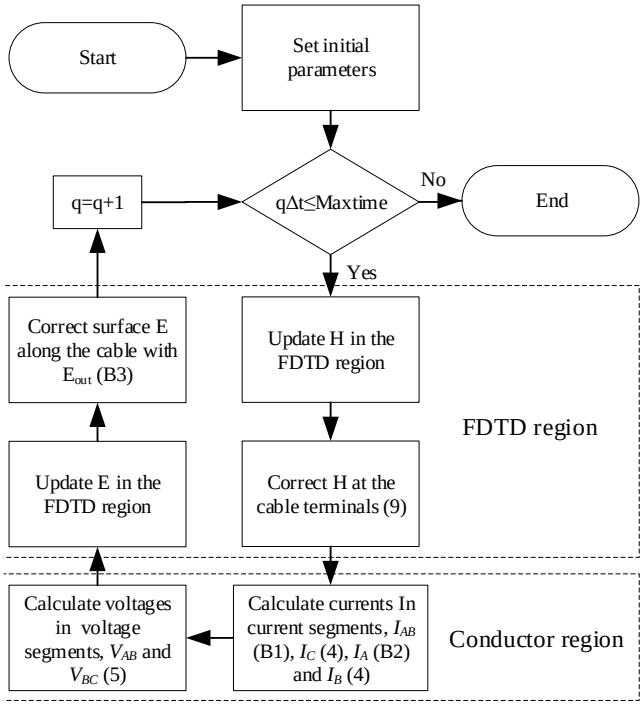

Fig. 4 Flow chart of the proposed lossy multilayer conductor model

D. *Computation procedure*

The computation procedure of the proposed multilayer coaxial conductor model is summarized in Fig. 4.

1) Update H field components in time step q, H^q, in the FDTD region as usual.
2) Correct H field components near cable terminals with (9). Note, $V_{AB}^{q-1/2}$ and $V_{BC}^{q-1/2}$ presented in (9) have been obtained in the previous step $q-1$.
3) Calculate I_t^q in current segments by integrating H field components in the FDTD region, and currents I_{AB}^q, I_C^q, I_A^q and I_B^q in the conductor region with (B1), (B2) and (4) in sequence.
4) Calculate voltages $V_{AB}^{q+1/2}$ and $V_{BC}^{q+1/2}$ in voltage segments in the conductor region with (5).
5) Update E field components, $E^{q+1/2}$, in the FDTD region as usual.
6) Replace surface E field components along the cable with $E_{out}^{q+1/2}$ obtained with (B3) for updating H field components in the FDTD region

III. VALIDATIONS

In this section, the proposed thin-wire model is validated analytically and numerically. For validation purpose, the

conductivity, relative permittivity and relative permeability of three conductors are assumed to be 1e6 S/m, 1 and 1, respectively. The relative permittivity of the insulation materials in the cable is assumed to 1. Various conductor radii of the cable are given in Table 2.

Table 2 Radii of the single-core cable with three metallic layers

Parameter	r_a	r_b	r_c	r_d	r_e
Radius / mm	2	2.5	2.7	3.3	3.5

A. *Analytical validation*

The configuration of a transmission line shown in Fig. 5 is adopted for the analytical validation of the proposed thin-wire model. A single-core cable has three-co-centric conductors as indicated in Table 2 and is arranged 0.04 m above a perfect ground. The left-side terminal is grounded via lossless wires and an ideal current source. This current source generates a sinusoidal waveform with an amplitude of 1 A and a frequency of 50 MHz or 100 MHz. Note that these frequencies are selected for efficient simulation and comparison.

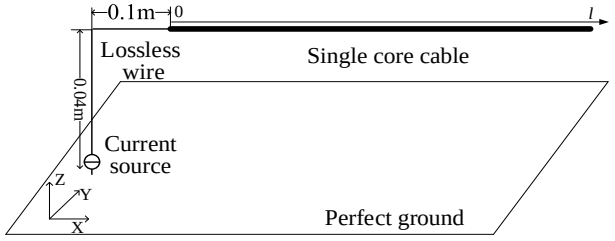

Fig. 5 Configuration of analytical validations

In the FDTD region, the working volume is $15.6\text{ m} \times 0.5\text{ m} \times 0.3\text{ m}$. Five perfectly matched layer (PML) absorbing boundaries [49] cover the working volume to absorb unwanted reflection. A perfect electric conductor (PEC) boundary is attached to the bottom of the working volume to simulate a perfect ground. The uniform mesh technique is adopted. The cell size and time step are defined as 0.01 m and 1.9245e-11 s. The current waveforms are recorded before the reflected waves arrive.

To validate the model analytically for the wave propagation in the single-core cable shown in Fig. 5, three coupled current updating equations with series impedances are constructed as

$$-\begin{bmatrix} \frac{dV_A}{dl} \\ \frac{dV_B}{dl} \\ \frac{dV_C}{dl} \end{bmatrix} = \begin{bmatrix} Z_{AA} & Z_{AB} & Z_{AC} \\ Z_{BA} & Z_{BB} & Z_{BC} \\ Z_{CA} & Z_{CB} & Z_{CC} \end{bmatrix} \times \begin{bmatrix} I_A \\ I_B \\ I_C \end{bmatrix}, \tag{11}$$

where V_X is the voltage difference between the conductor X (X = A, B or C) and the perfect ground. These phase-domain impedances in (11) are given in [50]. This model is adopted in EMTP for analyzing transients in a single-core cable with three co-centric conductors.

Since the shunt conductance of cable insulation is ignored, the voltage updating equations are expressed as

$$-\begin{bmatrix} \frac{dI_A}{dl} \\ \frac{dI_B}{dl} \\ \frac{dI_C}{dl} \end{bmatrix} = \begin{bmatrix} Y_{AA} & Y_{AB} & 0 \\ Y_{BA} & Y_{BB} & Y_{BC} \\ 0 & Y_{CB} & Y_{CC} \end{bmatrix} \times \begin{bmatrix} V_A \\ V_B \\ V_C \end{bmatrix}, \tag{12}$$

The phase-domain admittances in (12) are also given in [50]. Since the reflected waveforms are not recorded in the FDTD method, the cable in the EMTP is assumed to be semi-infinite. With (11) and (12), both currents and voltages are updated numerically using the approach given in [51]. For the validation purpose, the length of a cable segment and the time step of the TLT method are identical to the parameters used in the FDTD method.

There are three different cases of source connection to the cable, i.e., (a) conductor A, (b) conductor B and (c) conductor C. In each case, the current amplitudes at three locations along the cable are measured. The simulation results obtained from the TLT and proposed thin wire model (TWM) are shown in Tables 3 and 4 for comparison.

Table 3 Simulation results from TLT and proposed TWM (50 MHz)

Layers	Method	Current / A			Relative Error
		l=2m	*l*=4m	*l*=6m	
A	TLT	0.8648	0.7481	0.6472	0.31%
	TWM	0.8661	0.7503	0.6503	
B	TLT	0.8874	0.7883	0.7013	0.24%
	TWM	0.8891	0.7906	0.7030	
C	TLT	0.9966	0.9931	0.9897	0.15%
	TWM	0.9980	0.9947	0.9913	

Table 4 Simulation results from TLT and proposed TWM (100 MHz)

Layers	Method	Current / A			Relative Error
		l=2m	*l*=4m	*l*=6m	
A	TLT	0.8138	0.6642	0.5393	0.21%
	TWM	0.8134	0.6616	0.5383	
B	TLT	0.8438	0.7124	0.6020	0.06%
	TWM	0.8442	0.7126	0.6014	
C	TLT	0.9952	0.9904	0.9856	0.40%
	TWM	0.9990	0.9943	0.9897	

It is observed that the proposed thin-wire model is reasonably accurate. The averaged relative error is 0.23%. The maximum and minimum relative errors among these cases are 0.48% and 0.03%. The proposed thin-wire model can evaluate the frequency-dependent attenuation with acceptable accuracy.

B. *Numerical validation*

In this section, transients in the single-core coaxial cable are simulated with both the traditional FDTD method and the proposed thin-wire mode for comparison. Fig. 6 shows the configuration of the single-core cable for validation. For efficient computation with the traditional FDTD method, one 3-meter-long single-core cable is selected. It is placed 0.3 m above a perfect ground as shown in Fig. 6. Conductor C is grounded at its two ends via lossless wires. Conductor

B is left open at its two ends. One end of Conductor A is extended with a 0.1-meter-long wire and grounded via a lossless wire and a current source. The current source generates a 1 A Gaussian pulse waveform with parameters of σ=1e-9 s and μ=5e-9 s.

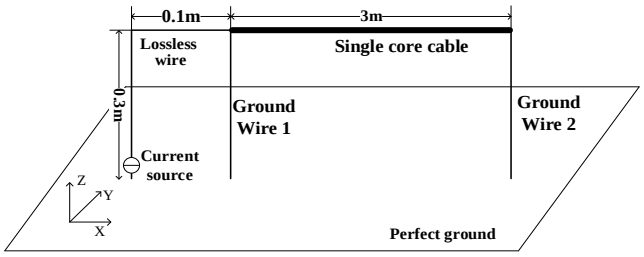

Fig. 6 Configuration of the single-core cable for numerical validations

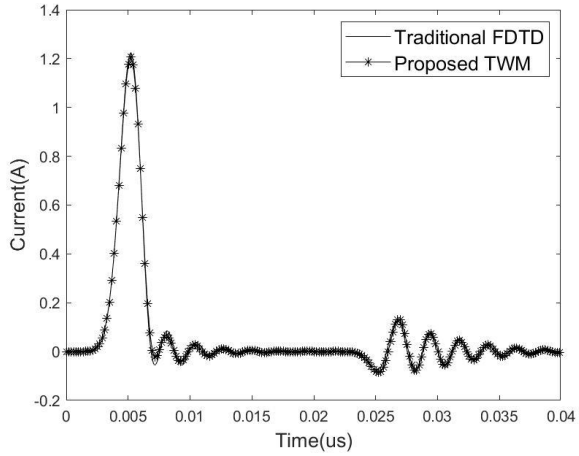

(a) Current waveform in Conductor A

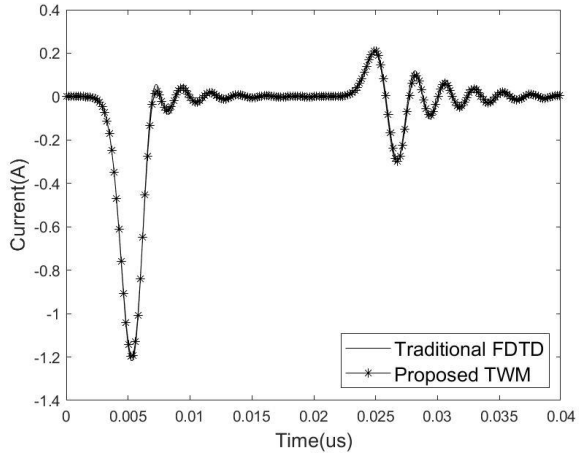

(b) Current waveform in Conductor C

Fig. 7 Current waveforms at the left side terminal of the cable are calculated with the traditional FDTD method (extremely dense FDTD mesh) and the proposed thin wire model (TWM)

In the simulation with the traditional FDTD method, the lossy cable is discretized with extremely dense FDTD mesh sizes to evaluate accurately the frequency-dependent loss. The working volume is set to be $4.5\text{m} \times 1\text{m} \times 1\text{m}$. Five PML boundaries and one PEC boundary enclose the whole working volume. The non-uniform mesh technique [52] is adopted. The cell size in the y and z directions near the cable is 0.03 mm and is increased to 10 mm gradually. The cell size in the x direction is set as 10 mm. The time step is defined as 6.1408e-14 s. While in the simulation with the proposed thin-wire model, the cell size (with a uniform meshing technique) and time step are set to be 10 mm and 1.9245e-11 s. In the simulation, the current waveforms at the left side terminal in Conductors A and C are measured.

A graphics processing unit (NVIDIA® Tesla™ K40C GPU Computing Accelerator) was used to accelerate numerical computation. The traditional FDTD method consumed 4.55 GB memory space and ran 12 hours and 41 minutes. While, the proposed method consumed 0.89 GB memory space and ran 4 minutes. Fig. 7 shows the currents on two conductors calculated with the traditional method and the proposed thin wire model under a pulse excitation. It is observed that current waveforms obtained from the proposed thin-wire model and traditional FDTD method match well in terms of waveshape and amplitude. The transients as well as the electromagnetic wave propagation on a lossy cable can be evaluated by the proposed thin-wire model with reasonable accuracy.

IV. Lightning Transients on an Underground Cable

The proposed thin wire model has been applied to analyze transients in a cable connection station under a lightning strike. The configuration of the station is shown in Fig. 8. A single-core insulated armored cable is buried 1 m below the ground. The length of the cable is 1 km and its radii are listed in Table 5. The rated voltages are 12.7 / 20 (24) kV. Its basic impulse level (BIL) is 144 kV. The metallic core and sheath are made of copper, and it is armored by aluminum wires. This cable is sheathed by polyvinyl chloride (PVC, $\varepsilon_r = 3$, $\mu_r = 1$, $\sigma = 0$) with 2.4 mm thickness. Cross-Linked Polyethylene (XLPE, $\varepsilon_r = 2.1$, $\mu_r = 1$, $\sigma = 0$) is padded between core, sheath and armor as insulation layers. The sheath and armor are shorted and grounded at both terminals. The grounding resistance of two grounding meshes is 3 ohm. Lightning arresters (LA) are provided to protect the cable and its associated equipment. The core conductor is connected to the overhead line at the left terminal. A concrete pole upholds the overhead line 10 m above ground. The right terminal of the core conductor is extended to a gas-insulated substation (GIS). The conductivity, relative permittivity and permeability of earth are 0.01 S/m, 4 and 1. The overhead line is struck by lightning directly.

Table 5 Radii of the single-core cable with three metallic layers

Parameter	r_a	r_b	r_c	r_d	r_e
Radius / mm	9.2	12.2	12.4	15.4	17.4

In the FDTD working volume, the cell size varies from 0.5 m (near the XLPE cable) to 10 m gradually. Six PML boundaries cover the working volume to absorb unwanted reflection. The time step is defined as 9.6225e-10 s. The lightning channel is simulated as a phased-current-source array in air [53]. A 2/70 μs waveform [54] with 100 kA amplitude is adopted. The LAs are modeled as active current sources by the piecewise linear method [55]. The residual

voltage is set as 50 kV. Surge currents and voltages in the middle of the cable are measure and shown in Fig. 9. The peak of the surge current in the core conductor is 19.87 kA. The induced sheath current has a similar waveform with opposite polarity. It is noticed that the majority of the lightning current is discharged to the earth via the grounding mesh. The peak voltage between the sheath and armour conductors is 361.14 kV, which is larger than the basic impulse insulation level, and may lead to insulation breakdown.

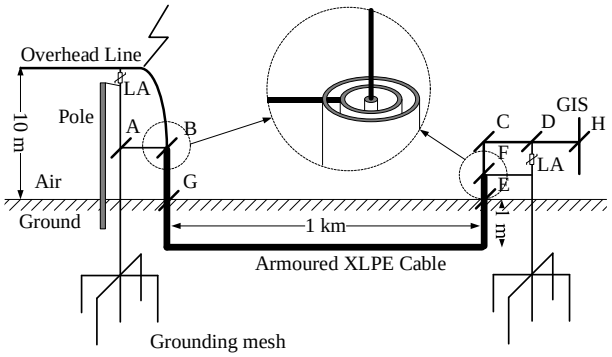

Fig. 8 The configuration of a cable connection station (L_{AB}=2.5m, L_{BG}=5m, L_{EF}=0m, L_{CE}=3m, L_{CD}=2.5m, L_{DH}=0m)

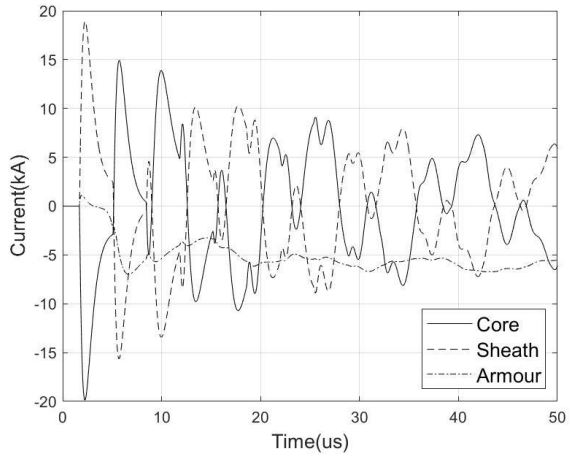

(a) Current waveforms

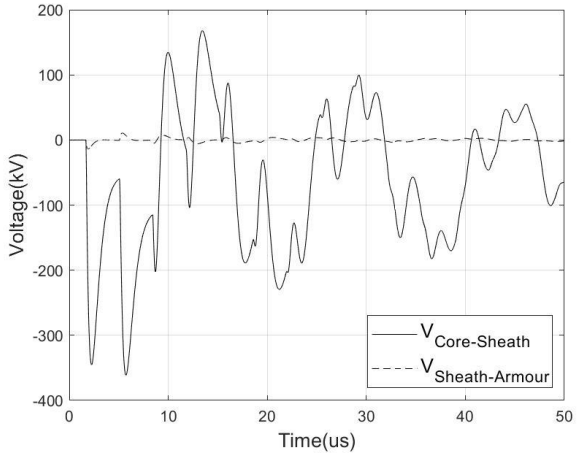

(b) Voltage waveforms

Fig. 9 Lightning surges at the middle of the underground cable

A sensitivity study of lightning surges against the lengths of segment AB, BG, CE and DH was performed. The maximum voltages between the core and sheath conductors in the middle of the cable were calculated with different segment lengths, and are listed in Table 6. The surge voltage amplitude reduces with decreasing the length of segment AB and increasing the length of segment BG. However, the length of segments at the GIS has a limited influence on the surge voltage.

Table 6 Maximum voltages in the middle of the cable between the core and sheath conductors with different segment lengths

Segment	Voltage / kV		
AB	Length=2.5m	Length =5m	Length =7.5m
	361.14	445.40	514.59
BG	Length =0m	Length =5m	Length =9m
	439.70	361.14	245.17
CE	Length =3m	Length =6m	Length =9m
	361.14	361.14	361.14
DH	Length =0m	Length =5m	Length =10m
	361.14	361.14	361.14

V. CONCLUSIONS

In this paper, a stable, matrix-free and efficient thin-wire model is proposed to simulate lossy single-core coaxial cables with three or more conductors. The whole working volume is divided into an FDTD region and a conductor region. To avoid matrix manipulations during each updating procedure, the multilayer cable is regarded as a series of coaxial transmission lines. The multiple transmission line equations are reduced to a series of classical 2-conductor transmission line equations. Unlike the c TLT, these lines may carry unbalanced currents, and the unbalanced current may not return via a conductive path. The electromagnetic fields in the FDTD region are updated with the traditional FDTD method. The frequency-dependent surface impedances of the cable are fully considered with the Bessel functions and approximated with the vector fitting technique for the time-domain simulation.

The proposed thin-wire model is validated with the TLT analytically and the traditional FDTD numerically. Both the amplitude and waveshape of the transients obtained with the proposed thin-wire model are reasonably accurate, compared to the simulation results obtained from other methods. Finally, the proposed model is applied to analyze surge behaviors in a cable connection station under a direct lightning stroke. It is found that the surge voltage between the core and sheath conductors is relatively high which may lead to insulation breakdown. By reducing the length of segment AB and increasing the length of segment BG, the surge voltage can be reduced during a lightning stroke to the OHL.

ACKNOWLEDGMENT

The work leading to this paper was supported by grants from the Research Grants Council of the HKSAR (Project No. 152100/17E and 152080/19E) and the Research Committee of the HK PolyU.

APPENDIX A

Consider a coaxial cable with three conductors as illustrated in Fig. 1. With the definition of the surface E field over conductor current, surface impedance $Z_{x,Y}$ (x=a, b, c, d or e, and Y=A, B, AB or C) on the surface at $r = r_x$ contributed by source current in Y is represented as [56],

$$Z_{a.A} = \frac{j\omega\mu_A}{2\pi R_a}\cdot\frac{I_0(R_a)}{I_1(R_a)},$$

$$Z_{b,A} = j\omega\mu_B\left[\begin{array}{l}\dfrac{[K_1(R_b)R_b - K_1(R_c)R_c]I_0(R_b)}{2\pi R_b R_c[I_1(R_c)K_1(R_b) - I_1(R_b)K_1(R_c)]}\\ -\dfrac{[I_1(R_c)R_c - I_1(R_b)R_b]K_0(R_b)}{2\pi R_b R_c[I_1(R_c)K_1(R_b) - I_1(R_b)K_1(R_c)]}\end{array}\right],$$

$$Z_{b.B} = j\omega\mu_B\frac{1}{2\pi R_b R_c[I_1(R_c)K_1(R_b) - I_1(R_b)K_1(R_c)]},$$

$$Z_{c.A} = j\omega\mu_B\left[\begin{array}{l}\dfrac{[K_1(R_b)R_b - K_1(R_c)R_c]I_0(R_c)}{2\pi R_b R_c[I_1(R_c)K_1(R_b) - I_1(R_b)K_1(R_c)]}\\ -\dfrac{[I_1(R_c)R_c - I_1(R_b)R_b]K_0(R_c)}{2\pi R_b R_c[I_1(R_c)K_1(R_b) - I_1(R_b)K_1(R_c)]}\end{array}\right],$$

$$Z_{c.B} = j\omega\mu_B\frac{K_1(R_b)I_0(R_c) + I_1(R_b)K_0(R_c)}{2\pi R_c[I_1(R_c)K_1(R_b) - I_1(R_b)K_1(R_c)]},$$

$$Z_{d,AB} = j\omega\mu_C\left[\begin{array}{l}\dfrac{[K_1(R_d)R_d - K_1(R_e)R_e]I_0(R_d)}{2\pi R_d R_e[I_1(R_e)K_1(R_d) - I_1(R_d)K_1(R_e)]}\\ -\dfrac{[I_1(R_e)R_e - I_1(R_d)R_d]K_0(R_d)}{2\pi R_d R_e[I_1(R_e)K_1(R_d) - I_1(R_d)K_1(R_e)]}\end{array}\right],$$

$$Z_{d.C} = j\omega\mu_C\frac{1}{2\pi R_e R_d[I_1(R_e)K_1(R_d) - I_1(R_d)K_1(R_e)]},$$

$$Z_{e.AB} = j\omega\mu_C\left[\begin{array}{l}\dfrac{[K_1(R_d)R_d - K_1(R_e)R_e]I_0(R_e)}{2\pi R_d R_e[I_1(R_e)K_1(R_d) - I_1(R_d)K_1(R_e)]}\\ -\dfrac{[I_1(R_e)R_e - I_1(R_d)R_d]K_0(R_e)}{2\pi R_d R_e[I_1(R_e)K_1(R_d) - I_1(R_d)K_1(R_e)]}\end{array}\right],$$

$$Z_{e.C} = j\omega\mu_C\frac{K_1(R_d)I_0(R_e) + I_1(R_d)K_0(R_e)}{2\pi R_e[I_1(R_e)K_1(R_d) - I_1(R_d)K_1(R_e)]},$$

where $R_x = mr_x$ and $m^2 = j\omega\mu(\sigma + j\omega\epsilon)$. Parameters μ, ε and σ are the permeability, permittivity and conductivity of the conductor, respectively. I_n is the modified Bessel function of the first kind at order n.

APPENDIX B

The discrete updating equation of I_{AB} in time domain can be derived as

$$\begin{aligned}I_{AB}^q = {} & C_{IAB}\cdot I_{AB}^{q-1} + C_{Itn}\cdot I_t^q + C_{Itp}\cdot I_t^{q-1} + C_{IAp1}\cdot I_A^{q-1} + C_{IAp2}\cdot I_A^{q-2}\\ & + C_{IBp1}\cdot I_B^{q-1} + C_{IBp2}\cdot I_B^{q-2} + C_{VBC}\cdot\partial V_{BC}^{q-1}/\partial l\\ & + \sum_{m=1}^{N}\left(\begin{array}{l}C_{d.AB.m}\cdot\varphi_{d.AB.m}^{q-1} + C_{d.C.m}\cdot\varphi_{d.C.m}^{q-1}\\ + C_{d.t.m}\cdot\varphi_{d.t.m}^{q-1} + C_{A.m}\cdot\varphi_{A.m}^{q-1} + C_{B.m}\cdot\varphi_{B.m}^{q-1}\end{array}\right),\end{aligned} \tag{B1}$$

where

$$\begin{aligned}D_{IAB} = {} & (-d_{d.AB} + d_{d.C})/2 + (L_{BC} - h_{d.AB} + h_{d.C})/\Delta t\\ & + \frac{1}{2}\sum_{m=1}^{N}(-B_{d.AB.m} + B_{d.C.m}),\end{aligned}$$

$$C_{IAB} = \left[(d_{d.AB} - d_{d.C})/2 + (L_{BC} - h_{d.AB} + h_{d.C})/\Delta t\right]/D_{IAB},$$

$$C_{Itn} = \left(\frac{d_{d.C}}{2} + \frac{h_{d.C}}{\Delta t} + \frac{1}{2}\sum_{m=1}^{N}B_{d.C.m}\right)\Big/D_{IAB},$$

$$C_{Itp} = (d_{d.C}/2 - h_{d.C}/\Delta t)/D_{IAB},$$

$$C_{IAp1} = -(d_{c.A} + h_{c.A}/\Delta t)/D_{IAB},$$

$$C_{IAp2} = h_{c.A}/(\Delta t\cdot D_{IAB}),$$

$$C_{IBp1} = -(d_{c.B} + h_{c.B}/\Delta t)/D_{IAB},$$

$$C_{IBp2} = h_{c.B}/(\Delta t\cdot D_{IAB}),$$

$$C_{VBC} = C_{A.m} = C_{B.m} = -1/D_{IAB},$$

$$C_{d.AB.m} = \left(e^{a_{d.AB.m}\cdot\Delta t} + 1\right)/(2\cdot D_{IAB}),$$

$$C_{d.C.m} = -\left(e^{a_{d.C.m}\cdot\Delta t} + 1\right)/(2\cdot D_{IAB}),$$

$$C_{t.m} = \left(e^{a_{d.C.m}\cdot\Delta t} + 1\right)/(2\cdot D_{IAB}).$$

The convolutional terms, $\varphi_{x.y.m}$, are updated in each updating procedure. The updating equations are listed as

$$\varphi_{d.AB.m}^q = B_{d.AB.m}\cdot I_{AB}^q + e^{a_{d.AB.m}\cdot\Delta t}\cdot\varphi_{d.AB.m}^{q-1},$$

$$\varphi_{d.C.m}^q = B_{d.C.m}\cdot I_{AB}^q + e^{a_{d.C.m}\cdot\Delta t}\cdot\varphi_{d.C.m}^{q-1},$$

$$\varphi_{t.m}^q = B_{d.C.m}\cdot I_t^q + e^{a_{d.C.m}\cdot\Delta t}\cdot\varphi_{t.m}^{q-1},$$

$$\varphi_{A.m}^q = B_{c.A.m}\cdot I_A^q + e^{a_{c.A.m}\cdot\Delta t}\cdot\varphi_{A.m}^{q-1},$$

$$\varphi_{B.m}^q = B_{c.B.m}\cdot I_B^q + e^{a_{c.B.m}\cdot\Delta t}\cdot\varphi_{B.m}^{q-1},$$

where $B_{x.Y.m} = r_{x.Y.m}/a_{x.Y.m}\cdot\left(e^{a_{x.Y.m}\cdot\Delta t} - 1\right)$.

The updating equation of I_A can be derived as

$$\begin{aligned}I_A^q = {} & C_{IA}\cdot I_A^{q-1} + C_{IABn}\cdot I_{AB}^q + C_{IABp}\cdot I_{AB}^{q-1} + C_{VAB}\cdot\partial V_{AB}^{q-1/2}/\partial l\\ & + \sum_{m=1}^{N}\left(\begin{array}{l}C_{a.A.m}\cdot\varphi_{a.A.m}^{q-1/2} + C_{b.A.m}\cdot\varphi_{b.A.m}^{q-1/2}\\ + C_{b.B.m}\cdot\varphi_{b.B.m}^{q-1/2} + + C_{AB.m}\cdot\varphi_{AB.m}^{q-1/2}\end{array}\right),\end{aligned} \tag{B2}$$

where

$$\begin{aligned}D_{IA} = {} & (d_{a.A} - d_{b.A} + d_{b.B})/2 + (L_{AB} + h_{a.A} - h_{b.A} + h_{b.B})/\Delta t\\ & + \frac{1}{2}\sum_{m=1}^{N}(B_{a.A.m} - B_{b.A.m} + B_{b.B.m}),\end{aligned}$$

$$C_{IA} = -\left[\begin{array}{l}(d_{a.A} - d_{b.A} + d_{b.B})/2\\ +(L_{AB} + h_{a.A} - h_{b.A} + h_{b.B})/\Delta t\end{array}\right]\Big/D_{IA},$$

$$C_{IABn} = \left(\frac{d_{b.B}}{2} + \frac{h_{b.B}}{\Delta t} + \frac{1}{2}\sum_{m=1}^{N}B_{b.B.m}\right)\Big/D_{IA},$$

$$C_{IABp} = (d_{b.B}/2 - h_{b.B}/\Delta t)/D_{IA},$$

$$C_{VAB} = -1/D_{IA},$$

$$C_{a.A.m} = -\left(e^{a_{a.A.m}\cdot\Delta t} + 1\right)/(2\cdot D_{IA}),$$

$$C_{b.A.m} = \left(e^{a_{b.A.m}\cdot\Delta t} + 1\right) \Big/ \left(2 \cdot D_{IA}\right),$$
$$C_{b.B.m} = -\left(e^{a_{b.B.m}\cdot\Delta t} + 1\right) \Big/ \left(2 \cdot D_{IA}\right),$$
$$C_{AB.m} = \left(e^{a_{b.B.m}\cdot\Delta t} + 1\right) \Big/ \left(2 \cdot D_{IA}\right).$$

The updating equations of convolutional terms in (16) are expressed as

$$\varphi^{q}_{a.A.m} = B_{a.A.m} \cdot I^{q}_{A} + e^{a_{a.A.m}\cdot\Delta t} \cdot \varphi^{q-1}_{a.A.m},$$
$$\varphi^{q}_{b.A.m} = B_{b.A.m} \cdot I^{q}_{A} + e^{a_{b.A.m}\cdot\Delta t} \cdot \varphi^{q-1}_{b.A.m},$$
$$\varphi^{q}_{b.B.m} = B_{b.B.m} \cdot I^{q}_{A} + e^{a_{b.B.m}\cdot\Delta t} \cdot \varphi^{q-1}_{b.B.m},$$
$$\varphi^{q}_{AB.m} = B_{b.B.m} \cdot I^{q}_{AB} + e^{a_{b.B.m}\cdot\Delta t} \cdot \varphi^{q-1}_{AB.m}.$$

The updating equation of E_{out} in the time domain is derived from (18) as

$$E^{q+1/2}_{out} = C_{ECn} \cdot I^{q}_{C} + C_{ECp} \cdot I^{q-1}_{C} + C_{EABn} \cdot I^{q}_{AB} + C_{EABp} \cdot I^{q-1}_{AB} + \sum_{m=1}^{N} \left(\varphi^{q}_{e.C.m} + \varphi^{q}_{e.AB.m}\right), \quad \text{(B3)}$$

Where

$$C_{ECn} = d_{e.C} + h_{e.C} / \Delta t,$$
$$C_{ECp} = -h_{e.C} / \Delta t,$$
$$C_{EABn} = d_{e.AB} + h_{e.AB} / \Delta t,$$
$$C_{EABp} = -h_{e.AB} / \Delta t.$$

The updating equations of convolutional terms are listed as

$$\varphi^{q}_{e.C.m} = B_{e.C.m} \cdot I^{q}_{C} + e^{a_{e.C.m}\cdot\Delta t} \cdot \varphi^{q-1}_{e.C.m},$$
$$\varphi^{q}_{e.AB.m} = B_{e.AB.m} \cdot I^{q}_{AB} + e^{a_{e.AB.m}\cdot\Delta t} \cdot \varphi^{q-1}_{e.AB.m}.$$

REFERENCES

[1] Roservear, R., *Power cables in 21st century energy development.* IEEE Power Engineering Review, 2000. **20**(9): p. 8-10.

[2] Marti, L., *Simulation of transients in underground cables with frequency-dependent modal transformation matrices.* IEEE Transactions on Power delivery, 1988. **3**(3): p. 1099-1110.

[3] Vance, E.F., *Coupling to shielded cables*. 1978: Wiley.

[4] Ametani, A., *A general formulation of impedance and admittance of cables.* IEEE Transactions on Power Apparatus and Systems, 1980(3): p. 902-910.

[5] Wedepohl, L. and D. Wilcox. *Transient analysis of underground power-transmission systems. System-model and wave-propagation characteristics*. in *Proceedings of the institution of electrical engineers*. 1973. IET.

[6] Orlandi, A. and C.R.J.I.T.o.e.c. Paul, *FDTD analysis of lossy, multiconductor transmission lines terminated in arbitrary loads.* IEEE Transactions on Electromagnetic Compatibility, 1996. **38**(3): p. 388-399.

[7] Celozzi, S. and M. Feliziani. *FDTD analysis of the interaction between a transient EM field and a lossy shielded cable*. in *Proc. 10th Int. Zurich Symp. EMC*. 1993.

[8] Gustavsen, B. and A. Semlyen, *Simulation of transmission line transients using vector fitting and modal decomposition.* IEEE Transactions on Power Delivery, 1998. **13**(2): p. 605-614.

[9] Gustavsen, B. and A. Semlyen, *Rational approximation of frequency domain responses by vector fitting.* IEEE Transactions on Power Delivery, 1999. **14**(3): p. 1052-1061.

[10] Yu, T.-C. and J.R. Martí, *A robust phase-coordinates frequency-dependent underground cable model (zCable) for the EMTP.* IEEE Transactions on Power Delivery, 2003. **18**(1): p. 189-194.

[11] Ametani, A., *A highly efficient method for calculating transmission line transients.* IEEE Transactions on Power Apparatus and Systems, 1976. **95**(5): p. 1545-1551.

[12] Gustavsen, B., J. Sletbak, and T. Henriksen, *Calculation of electromagnetic transients in transmission cables and lines taking frequency dependent effects accurately into account.* IEEE Transactions on Power Delivery, 1995. **10**(2): p. 1076-1084.

[13] Semlyen, A. and A. Dabuleanu, *Fast and accurate switching transient calculations on transmission lines with ground return using recursive convolutions.* IEEE Transactions on Power Apparatus and Systems, 1975. **94**(2): p. 561-571.

[14] Aguet, M., M. Ianovici, and C.-C.J.I.T.o.E.C. Lin, *Transient electromagnetic field coupling to long shielded cables.* IEEE Transactions on Electromagnetic Compatibility, 1980. **22**(4): p. 276-282.

[15] D'Amore, M. and M. Feliziani. *EMP coupling to coaxial shielded cables*. in *International Symposium on Electromagnetic Compatibility*. 1988. IEEE.

[16] D'Amore, M. and M. Feliziani. *Induced fast transients in multiconductor shielded cables*. in *Seventh International Conference on Electromagnetic Compatibility,* 1990. IET.

[17] Umashankar, K., et al., *Calculation and experimental validation of induced currents on coupled wires in an arbitrary shaped cavity.* IEEE Transactions on Antennas and Propagation, 1987. **35**(11): p. 1248-1257.

[18] Feliziani, M. and F.J.I.t.o.m. Maradei, *Field-to-wire coupling using the finite element-time domain (FE-TD) method.* IEEE Transactions on Magnetics, 1995. **31**(3): p. 1586-1589.

[19] Berenger, J.-P., *A multiwire formalism for the FDTD method.* IEEE Transactions on Electromagnetic Compatibility, 2000. **42**(3): p. 257-264.

[20] Feliziani, M. and F.J.I.t.o.m. Maradei, *Full-wave analysis of shielded cable configurations by the FDTD method.* IEEE transactions on magnetics, 2002. **38**(2): p. 761-764.

[21] Agrawal, A.K., H.J. Price, and S.H. Gurbaxani, *Transient response of multiconductor transmission lines excited by a nonuniform electromagnetic field.* IEEE Transactions on electromagnetic compatibility, 1980(2): p. 119-129.

[22] Yee, K.S., *Numerical solution of initial boundary value problems involving Maxwell's equations in isotropic media.* IEEE Transactions on Antennas Propagation, 1966. **14**(3): p. 302-307.

[23] Holland, R. and L. Simpson, *Finite-difference analysis of EMP coupling to thin struts and wires.* IEEE Transactions on Electromagnetic Compatibility, 1981(2): p. 88-97.

[24] Taflove, A., et al., *Detailed FD-TD analysis of electromagnetic fields penetrating narrow slots and lapped joints in thick conducting screens.* IEEE Transactions on Antennas and Propagation, 1988. **36**(2): p. 247-257.

[25] Noda, T. and S. Yokoyama, *Thin wire representation in finite difference time domain surge simulation.* IEEE Transactions on Power Delivery, 2002. **17**(3): p. 840-847.

[26] Railton, C.J., et al., *The treatment of geometrically small structures in FDTD by the modification of assigned material parameters.* IEEE Transactions on Antennas and Propagation, 2005. **53**(12): p. 4129-4136.

[27] Xiong, R., et al., *Optimized programs for shaped conductive backfill material of grounding systems based on the FDTD simulations.* IEEE Transactions on Power Delivery, 2014. **29**(4): p. 1744-1751.

[28] Musa, B.U., W.H. Siew, and M.D. Judd, *Computation of transient electromagnetic fields due to switching in high-voltage substations.* IEEE Transactions on Power Delivery, 2010. **25**(2): p. 1154-1161.

[29] Rizk, M.E., et al., *Computation of Peak Lightning-Induced Voltages due to the Typical First and Subsequent Strokes Considering High Ground Resistivity.* IEEE Transactions on Power Delivery, 2016, 32(4): 1861-1871.

[30] Zhang, Q., et al., *An approximate formula for estimating the peak value of lightning-induced overvoltage considering the stratified conducting ground.* IEEE Transactions on Power Delivery, 2014. **29**(2): p. 884-889.

[31] Baba, Y. and V. Rakov, *Voltages induced on an overhead wire by lightning strikes to a nearby tall grounded object.* IEEE Transactions on Electromagnetic Compatibility, 2006. **48**(1): p. 212-224.

[32] Noda, T., *A numerical simulation of transient electromagnetic fields for obtaining the step response of a transmission tower using the*

FDTD method. IEEE Transactions on Power Delivery, 2008. **23**(2): p. 1262-1263.
[33] Goni, O., et al., *Simulation and experimental analyses of electromagnetic transients behaviors of lightning surge on vertical conductors.* IEEE Transactions on Power Delivery, 2006. **21**(4): p. 1778-1786.
[34] Du, Y., B. Li, and M. Chen, *Surges induced in building electrical systems during a lightning strike.* Electric Power Systems Research, 2016, 139: 68-74.
[35] Li, B., Y. Du, and M. Chen, *An FDTD Thin-Wire Model for Lossy Wire Structures With Noncircular Cross Section.* IEEE Transactions on Power Delivery, 2018. **33**(6): p. 3055-3064.
[36] Thang, T.H., et al., *FDTD simulation of insulator voltages at a lightning-struck tower considering ground-wire corona.* IEEE Transactions on Power Delivery, 2013. **28**(3): p. 1635-1642.
[37] Makinen, R. M., *An efficient surface-impedance boundary condition for thin wires of finite conductivity.* IEEE Transactions on Antennas and Propagation, 2004, **52**(12): 3364-3372.
[38] Fujita, K., *Modeling of beam-wall interaction in a finite-length metallic pipe with multiple surface perturbations.* IEEE Journal on Multiscale and Multiphysics Computational Techniques, 2017, 2: 237-242.
[39] Fujita, K., *Multiscale modeling of a short relativistic electron bunch interacting with long resistive structures at cryogenic temperatures.* IEEE Journal on Multiscale and Multiphysics Computational Techniques, 2016, 1: 107-119.
[40] Tatematsu, A., *A technique for representing coaxial cables for FDTD-based surge simulations.* IEEE Transactions on Electromagnetic Compatibility, , 2015. **57**(3): p. 488-495.
[41] Du, Y., B. Li, and M. Chen, *The Extended Thin-Wire Model of Lossy Round Wire Structures for FDTD Simulations.* IEEE Transactions on Power Delivery, 2017. **32**(6): p. 2472-2480.
[42] Tatematsu, A., *A Technique for Representing Lossy Thin Wires and Coaxial Cables for FDTD-Based Surge Simulations.* IEEE Transactions on Electromagnetic Compatibility, 2018. **60**(3): p. 705-715.
[43] Li, B., Y.P. Du, and M. Chen, *Thin-wire Models for Inclined Conductors with Frequency-dependent Losses.* IEEE Transactions on Power Delivery, 2019. **35**(3): p. 1083-1092.
[44] Gustavsen, B., J. Martinez, and D.J.I.T.o.p.d. Durbak, *Parameter determination for modeling system transients-Part II: Insulated cables.* IEEE Transactions on power delivery, 2005, **20**(3): 2045-2050.
[45] Mugala, G., et al., *Dependence of XLPE insulated power cable wave propagation characteristics on design parameters.* IEEE Transactions on dielectrics and electrical insulation, 2007, 14(2): 393-399.
[46] Gustavsen, B., *Improving the pole relocating properties of vector fitting.* IEEE Transactions on Power Delivery, 2006. **21**(3): p. 1587-1592.
[47] Gustavsen, B., *Fast passivity enforcement for pole-residue models by perturbation of residue matrix eigenvalues.* IEEE Transactions on Power Delivery, 2008. **23**(4): p. 2278-2285.
[48] Li, B., Y.P. Du, and M. Chen, *Thin-wire Models for Inclined Conductors with Frequency-dependent Losses.* IEEE Transactions on Power Delivery, 2019, **35**(3): 1083-1092.
[49] Berenger, J.-P., *A perfectly matched layer for the absorption of electromagnetic waves.* Journal of computational physics, 1994. **114**(2): p. 185-200.
[50] Dommel, H., *Electromagnetic transients program theory book.* Portland, prepared for BPA, 1986.
[51] Paul, C.R., *Analysis of multiconductor transmission lines*. 2007: John Wiley & Sons.
[52] Namiki, T. and K. Ito. *Accuracy improvement technique applied to non-uniform FDTD cells using high-order implicit scheme*. in *Antennas and Propagation Society International Symposium,* 2001. IEEE.
[53] Baba, Y. and V. Rakov, *On the transmission line model for lightning return stroke representation.* Geophysical Research Letters, 2003. **30**(24).
[54] Chang, H.-C., et al., *Energy dispatching analysis of lightning surges on underground cables in a cable connection station.* Energy conversion and management, 2011. **52**(1): p. 693-702.
[55] Tatematsu, A. and T. Noda, *Three-dimensional FDTD calculation of lightning-induced voltages on a multiphase distribution line with the lightning arresters and an overhead shielding wire.* IEEE Transactions on Electromagnetic Compatibility, 2014. **56**(1): p. 159-167.
[56] Schelkunoff, S.A., *The electromagnetic theory of coaxial transmission lines and cylindrical shields.* Bell Labs Technical Journal, 1934. **13**(4): p. 532-579.